# Passivity-based Motion and Force Tracking Control for Constrained Elastic Joint Robots

Meng, Xuming; Keppler, Manuel; Ott, Christian

# Passivity-based Motion and Force Tracking Control for Constrained Elastic Joint Robots

Xuming Meng, Manuel Keppler and Christian Ott, *Senior Member, IEEE*

***Abstract*— In the past, several motion and force controls were successfully implemented on rigid-joint robots with constraints. With the invention of mechanically compliant robots, the focus on designing controllers for elastic joint robots with constraints is increasing, especially involving the complexity of the joint elasticity in control. Aiming to bridge the gap between the control schemes of rigid- and elastic-joint robots, this letter presents a controller consisting of a PD+ task-space tracking and integral force control, while the intrinsic inertial and elastic properties of the system are fully preserved. We provide a passivity analysis and prove uniform asymptotic stability of the equilibrium. Simulations on a planar two-armed benchmark system with constraints validate the proposed control law.**

***Index Terms*— Robotics, control applications**

## I. Introduction

FOR the sake of improving the mechanical robustness while keeping structural rigidity, robot design has incorporated the joint elasticity progressively since the 90s. This joint elasticity, inspired by nature, provides many benefits, e.g., large impact tolerance and energy storage, etc. However, dealing with combined motion and force control problems is more challenging than for pure motion control, especially when the robot is constrained. The constrained robots can be seen as multi-body systems with closed-loop topologies, such as cooperative manipulation, robotic hands for grasping, or humanoid robots. Therefore, one question arises: how to control motion and force simultaneously and robustly on a constrained elastic joint robot?

In the domain of hybrid motion and force control for elastic joint robots, Spong [1] proposed the ideas of integral manifolds and corrective control for elastic joint manipulators in both constrained (motion) space and unconstrained (force) space. However, a fast inner control loop would be needed due to the assumed singularly perturbed system. Mills [2] had a similar approach. A corrective term was applied in the slow loop to compensate for the joint flexibility. More recently, Aghili [3] proposed a projected inverse-dynamic method for a rigid-joint robot. The controller design is based on separating the original dynamics into two independent orthogonal spaces. Mistry et al. [4], [5] extended this formulation to the operational space, which is used for underactuated robots, e.g., humanoid robots.

Since then, various variants of these projected methods were presented. The researchers in [6] conducted the experimental studies on the fully decoupling of motion and force control of a light-weight robot by formulating an explicit force controller. The general projection method, i.e., implementing inverse-dynamics controller in the constraint-free space and solving optimization problems in the constrained space, was successfully validated on multi-arm robots and quadrupeds for manipulation and locomotion tasks [7], [8].

Notwithstanding the effectiveness of the works mentioned above, the rigid joint controllers [3]–[8] cannot be directly implemented on elastic joint robots. One possible solution is to additionally design an inner loop (e.g., a cascaded or a two-loop structure in [1], [2]) after that. However, it inevitably shapes the original dynamics. Besides, in [3], [5], at least in one subspace (usually is the unconstrained space), an inverse-dynamics (feedback-linearization) controller is utilized, which consists of canceling out or modifying the intrinsic properties. Furthermore, the passivity feature is unclear;

Controlling robots through a passive design was illustrated in [9], [10]. Keppler et al. [11], [12] proposed a passive controller, aiming for imposing the desired interaction behavior on the either motor side or link side, while the intrinsic elastic properties remain unchanged. Following this idea, this letter aims to design a motion/force controller for the elastic joint robots, and contributions of this letter are

1) We propose a passivity-based controller for elastic joint robots that achieves simultaneous motion tracking and force control. We choose a dynamically consistent projector and preserve the robot's intrinsic inertial and elastic structure.
2) An integral force control is designed to solve a steady-state error problem in the case of constant disturbances in the constrained space. The output strict passivity for the physical interaction and uniform asymptotic stability for the free motion are shown.

## II. System Dynamics

We consider a robot dynamics model with all rotational joints implemented by Serial Elastic Actuators (SEAs). For the highly-geared actuators, we shall use the reduced model, proposed by Spong [13], with $n$ rigid links with $m$ linearly independent kinematic constraints[1], expressed by a set of

This work was supported by the European Research Council (ERC) under the European Union's Horizon 2020 research and innovation programme with grant agreement No. 819358 (Project: NatDyReL).

The authors are with the Institute of Robotics and Mechatronics, German Aerospace Center (DLR), Münchner Str. 20, 82234 Weßling, Germany (e-mail: xuming.meng@dlr.de; manuel.keppler@dlr.de)

Christian Ott is also with the Automation and Control Institute at TU Wien, 1040 Vienna, Austria (e-mail: christian.ott@tuwien.ac.at)

[1]In this work, we assume the constraint is holonomic.

algebraic equations [14]

$$\boldsymbol{M}(\boldsymbol{q})\ddot{\boldsymbol{q}} + \boldsymbol{C}(\boldsymbol{q},\dot{\boldsymbol{q}})\dot{\boldsymbol{q}} + \boldsymbol{g}(\boldsymbol{q}) = \boldsymbol{K}(\boldsymbol{\theta}-\boldsymbol{q}) + \boldsymbol{A}(\boldsymbol{q})^T\boldsymbol{\lambda} + \boldsymbol{\tau}_{ext}, \tag{1a}$$

$$\boldsymbol{B}\ddot{\boldsymbol{\theta}} + \boldsymbol{K}(\boldsymbol{\theta}-\boldsymbol{q}) = \boldsymbol{u}, \tag{1b}$$

$$\boldsymbol{A}(\boldsymbol{q})\dot{\boldsymbol{q}} = \boldsymbol{0}, \tag{1c}$$

where $\boldsymbol{q} \in \mathbb{R}^n$ represents link position. $\boldsymbol{M}(\boldsymbol{q})$ is a symmetric positive definite link inertia matrix, $\boldsymbol{C}(\boldsymbol{q},\dot{\boldsymbol{q}})$ the Coriolis/centrifugal matrix. $\boldsymbol{g}(\boldsymbol{q})$ denotes the gravity torque, $\boldsymbol{\tau}_{ext} \in \mathbb{R}^n$ the generalized external torques on the link, $\boldsymbol{\theta} \in \mathbb{R}^n$ the motor coordinate. The positive diagonal matrix $\boldsymbol{B}$ includes the reflected motor inertia, with the following assumptions

**Assumption 1.** *The singular values of inertia $\boldsymbol{M}(\boldsymbol{q})$ and $\boldsymbol{B}$ are bounded above and bounded below away from zero. Hence, both $\boldsymbol{M}(\boldsymbol{q})^{-1}$ and $\boldsymbol{B}^{-1}$ exist and are bounded. Besides, $\boldsymbol{C}(\boldsymbol{q},\dot{\boldsymbol{q}})$ is bounded in $\boldsymbol{q}$ and bounded for bounded $\dot{\boldsymbol{q}}$. $\dot{\boldsymbol{M}}(\boldsymbol{q}) - 2\boldsymbol{C}(\boldsymbol{q},\dot{\boldsymbol{q}})$ is skew-symmetric.*

The positive diagonal stiffness $\boldsymbol{K}$ represents a linear torsional spring connecting the link and motor shaft. The motor input $\boldsymbol{u} \in \mathbb{R}^n$ is the control input. $\boldsymbol{\lambda}$ is a Lagrange multiplier which denotes the constraint force. $\boldsymbol{A}(\boldsymbol{q}) \coloneqq \frac{\partial \boldsymbol{\phi}(\boldsymbol{q})}{\partial \boldsymbol{q}} \in \mathbb{R}^{m\times n}$ is a constraint Jacobian matrix, where $\boldsymbol{\phi}(\boldsymbol{q}) = \boldsymbol{0}, \mathbb{R}^n \to \mathbb{R}^m$ is a constraint function, with the following assumption:

**Assumption 2.** *The holonomic constraint $\boldsymbol{\phi}(\boldsymbol{q})$ is at least four times differentiable. The constraint Jacobian matrix $\boldsymbol{A}(\boldsymbol{q})$ has full rank $m$ and is uniformly bounded in $\boldsymbol{q}$.*

Due to kinematic constraints, $\boldsymbol{q}$ is not a minimal coordinate any more. The minimal generalized coordinates has dimension $n-m$. Authors in [3], [5] introduced a projection operator $\boldsymbol{P}$, such that[2] $\dot{\boldsymbol{q}} = \boldsymbol{P}\dot{\boldsymbol{q}}$, for all $\dot{\boldsymbol{q}}$ in the nullspace of $\boldsymbol{A}$. $\boldsymbol{P}$ is not unique. In order to preserve the original inertial properties, different from [3], [5], we choose a dynamically consistent projector, $\boldsymbol{P} = \boldsymbol{I} - \boldsymbol{A}^{M+}\boldsymbol{A}$, where $\boldsymbol{A}^{M+} = \boldsymbol{M}^{-1}\boldsymbol{A}^T(\boldsymbol{A}\boldsymbol{M}^{-1}\boldsymbol{A}^T)^{-1}$ is an inertia-weighted inverse. It also implies $\boldsymbol{A}\boldsymbol{P} = \boldsymbol{0}$, and the projector fulfills $\boldsymbol{P} = \boldsymbol{P}^2$.

In order to achieve a task-space tracking, we define a task space $\boldsymbol{x} \coloneqq \boldsymbol{f}(\boldsymbol{q})$, $\boldsymbol{f} : \mathbb{Q} \to \mathbb{R}^t$, where $\mathbb{Q} \subseteq \mathbb{R}^n$. The task-space velocity is expressed by

$$\dot{\boldsymbol{x}} = \boldsymbol{J}(\boldsymbol{q})\dot{\boldsymbol{q}} = \boldsymbol{J}(\boldsymbol{q})\boldsymbol{P}\dot{\boldsymbol{q}}\ , \tag{2}$$

where $\boldsymbol{J}(\boldsymbol{q}) = \partial \boldsymbol{f}(\boldsymbol{q})/\partial \boldsymbol{q} \in \mathbb{R}^{t\times n}$. Stacking the task-space mapping and constraints, and taking derivative, we have

$$\underbrace{\begin{bmatrix}\boldsymbol{0}\\ \boldsymbol{x}\end{bmatrix}}_{\bar{\boldsymbol{x}}} = \underbrace{\begin{bmatrix}\boldsymbol{\phi}(\boldsymbol{q})\\ \boldsymbol{f}(\boldsymbol{q})\end{bmatrix}}_{\bar{\boldsymbol{f}}(\boldsymbol{q})} \xrightarrow{\frac{\mathrm{d}}{\mathrm{d}t}} \underbrace{\begin{bmatrix}\boldsymbol{0}\\ \dot{\boldsymbol{x}}\end{bmatrix}}_{\dot{\bar{\boldsymbol{x}}}} = \underbrace{\begin{bmatrix}\boldsymbol{A}\\ \boldsymbol{J}\boldsymbol{P}\end{bmatrix}}_{\bar{\boldsymbol{J}}(\boldsymbol{q})}\dot{\boldsymbol{q}}\ , \tag{3}$$

where $\bar{\boldsymbol{x}}$, $\dot{\bar{\boldsymbol{x}}}$ and $\bar{\boldsymbol{f}}(\boldsymbol{q})$ are the extended task-space position, velocity and the mapping function including constraints, respectively. $\bar{\boldsymbol{J}}$ denotes the augmented task Jacobian matrix.

**Assumption 3.** *The mapping $\bar{\boldsymbol{f}}(\boldsymbol{q})$ is one-to-one in $\bar{\mathbb{Q}}$, where $\bar{\mathbb{Q}} \coloneqq \{\boldsymbol{q} \in \mathbb{Q} \mid \sigma_l < \sigma_m(\bar{\boldsymbol{J}}(\boldsymbol{q})) < \sigma_u\}$[3], where $\sigma_l$ and $\sigma_u$ are lower and upper bounds, respectively. It implies that the task space is free of singularities. Each task $x_i$ is independently defined, and also independent from each constraint $\phi_i(\boldsymbol{q})$. The extended task $\bar{\boldsymbol{x}}$ spans the remaining state space as a whole, i.e., $t = m-n$, $\bar{\boldsymbol{J}} \in \mathbb{R}^{n\times n}$ and $\mathrm{rank}(\bar{\boldsymbol{J}}) = n$. It is also assumed that $\bar{\boldsymbol{f}}(\boldsymbol{q})$ is continuously differentiable with $\boldsymbol{q}$.*

The singularity-free workspace is a common assumption for the analysis of task-space controllers [15]. Due to Assumption 3, $\bar{\boldsymbol{J}}(\boldsymbol{q})$ is invertible, and uniquely determined by $\bar{\boldsymbol{J}}^{-1} = \begin{bmatrix}\boldsymbol{A}^{M+} & \boldsymbol{P}(\boldsymbol{J}\boldsymbol{P})^+\end{bmatrix}$, where $\boldsymbol{P}(\boldsymbol{J}\boldsymbol{P})^+ = \boldsymbol{P}\boldsymbol{P}^T\boldsymbol{J}^T(\boldsymbol{J}\boldsymbol{P}\boldsymbol{P}^T\boldsymbol{J}^T)^{-1}$. Therefore, taking derivative of (3), we get the joint velocities $\dot{\boldsymbol{q}}$ and accelerations $\ddot{\boldsymbol{q}}$, respectively

$$\dot{\boldsymbol{q}} = \bar{\boldsymbol{J}}^{-1}\dot{\bar{\boldsymbol{x}}}, \qquad \ddot{\boldsymbol{q}} = \bar{\boldsymbol{J}}^{-1}\ddot{\bar{\boldsymbol{x}}} - \bar{\boldsymbol{J}}^{-1}\dot{\bar{\boldsymbol{J}}}\bar{\boldsymbol{J}}^{-1}\dot{\bar{\boldsymbol{x}}}. \tag{4}$$

Substitute (4) into (1a) and multiply $\bar{\boldsymbol{J}}^{-T}$ on the left, we have the task-space dynamics

$$\boldsymbol{\Lambda}(\boldsymbol{q})\ddot{\bar{\boldsymbol{x}}} + \boldsymbol{\mu}(\boldsymbol{q},\dot{\boldsymbol{q}})\dot{\bar{\boldsymbol{x}}} = \bar{\boldsymbol{J}}^{-T}[\boldsymbol{K}(\boldsymbol{\theta}-\boldsymbol{q}) - \boldsymbol{g} + \boldsymbol{A}^T\boldsymbol{\lambda} + \boldsymbol{\tau}_{ext}]. \tag{5}$$

Thank to the structure of $\bar{\boldsymbol{J}}$, the transformed inertia matrix $\boldsymbol{\Lambda} = \mathrm{diag}(\boldsymbol{\Lambda}_{cc}, \boldsymbol{\Lambda}_{xx}) = \bar{\boldsymbol{J}}^{-T}\boldsymbol{M}\bar{\boldsymbol{J}}^{-1}$ is block-diagonal, and the Coriolis/centrifugal matrix is expressed by $\boldsymbol{\mu} = \begin{bmatrix}\boldsymbol{\mu}_{cc} & \boldsymbol{\mu}_{cx}\\ \boldsymbol{\mu}_{xc} & \boldsymbol{\mu}_{xx}\end{bmatrix} = \bar{\boldsymbol{J}}^{-T}\big(-\boldsymbol{M}\bar{\boldsymbol{J}}^{-1}\dot{\bar{\boldsymbol{J}}} + \boldsymbol{C}\big)\bar{\boldsymbol{J}}^{-1}$. Note that we have the properties of $\dot{\boldsymbol{\Lambda}}_{xx} = \boldsymbol{\mu}_{xx} + \boldsymbol{\mu}_{xx}^T$ and $\boldsymbol{\mu}_{cx} = -\boldsymbol{\mu}_{xc}^T$, cf. [16, Sec. 4.4] for details. We separate the open-loop dynamics (5) in constrained and unconstrained spaces, i.e.,

$$\boldsymbol{\lambda} = \boldsymbol{\mu}_{cx}\dot{\bar{\boldsymbol{x}}} - (\boldsymbol{A}^{M+})^T\big[\boldsymbol{K}(\boldsymbol{\theta}-\boldsymbol{q}) - \boldsymbol{g}\big] - \boldsymbol{\lambda}_{ext}, \tag{6a}$$

$$\boldsymbol{\Lambda}_{xx}\ddot{\bar{\boldsymbol{x}}} + \boldsymbol{\mu}_{xx}\dot{\bar{\boldsymbol{x}}} = [\boldsymbol{P}(\boldsymbol{J}\boldsymbol{P})^+]^T\big[\boldsymbol{K}(\boldsymbol{\theta}-\boldsymbol{q}) - \boldsymbol{g}\big] + \boldsymbol{F}_{ext}. \tag{6b}$$

Note that the generalized external torque $\boldsymbol{\tau}_{ext}$ in the joint space fulfills $\boldsymbol{\tau}_{ext} = \boldsymbol{A}^T\boldsymbol{\lambda}_{ext} + (\boldsymbol{J}\boldsymbol{P})^T\boldsymbol{F}_{ext}$ where $\mathcal{C}^1$-continuous $\boldsymbol{F}_{ext}$ denotes disturbance in the unconstrained space and $\mathcal{C}^1$-continuous $\boldsymbol{\lambda}_{ext}$ in the constrained space.

## III. Control Objectives and Design

Our objective is to achieve simultaneously (i) a passive, asymptotic task-space motion tracking; (ii) a force tracking control, capable of rejecting constant disturbances; (iii) preserving the intrinsic elastic and the inertial properties.

### A. Desired Closed-loop Dynamics

The philosophy of a passive design follows the one in the previous work [12] similarly, called Elastic Structure Preserving (ESP) control, which facilitates an underactuated robot to a quasi fully-actuated system. The reference motion $\boldsymbol{x}_d(t)$ and force trajectory $\boldsymbol{\lambda}_d(t)$ satisfy the following assumption.

**Assumption 4.** *The reference motion trajectory $\boldsymbol{x}_d(t) \in \mathcal{C}^4$ is assumed with bounded $\|\dot{\boldsymbol{x}}_d(t)\|$, ..., $\|\boldsymbol{x}_d^{(4)}(t)\|$, and the reference force trajectory $\boldsymbol{\lambda}_d(t) \in \mathcal{C}^2$ with bounded $\|\dot{\boldsymbol{\lambda}}_d(t)\|$, $\|\ddot{\boldsymbol{\lambda}}_d(t)\|$.*

We present our desired closed-loop dynamics:

$$\tilde{\boldsymbol{\lambda}} = -\boldsymbol{K}_I\int_0^t \tilde{\boldsymbol{\lambda}}(\tau)\mathrm{d}\tau - (\boldsymbol{A}^{M+})^T\boldsymbol{K}(\boldsymbol{\eta} - \boldsymbol{G}(\tilde{\boldsymbol{x}})) + \boldsymbol{\mu}_{cx}\dot{\tilde{\boldsymbol{x}}} - \boldsymbol{\lambda}_{ext}, \tag{7a}$$

$$\boldsymbol{\Lambda}_{xx}\ddot{\tilde{\boldsymbol{x}}} + (\boldsymbol{\mu}_{xx} + \boldsymbol{D}_x)\dot{\tilde{\boldsymbol{x}}} + \boldsymbol{K}_x\tilde{\boldsymbol{x}} = [\boldsymbol{P}(\boldsymbol{J}\boldsymbol{P})^+]^T\boldsymbol{K}(\boldsymbol{\eta} - \boldsymbol{G}(\tilde{\boldsymbol{x}})) + \boldsymbol{F}_{ext}, \tag{7b}$$

$$\boldsymbol{B}\ddot{\boldsymbol{\eta}} + \boldsymbol{K}(\boldsymbol{\eta} - \boldsymbol{G}(\tilde{\boldsymbol{x}})) = -\boldsymbol{D}_\eta\dot{\boldsymbol{\eta}}, \tag{7c}$$

[2] For easy notation, we omit the argument $\boldsymbol{q}$ in $\boldsymbol{P}(\boldsymbol{q})$, same for $\boldsymbol{J}$, $\bar{\boldsymbol{J}}$.

[3] In the following text, $\sigma_m(\boldsymbol{A})$ (or: $\lambda_m(\boldsymbol{A})$), $\sigma_M(\boldsymbol{A})$ (or: $\lambda_M(\boldsymbol{A})$) represent the minimal and maximal singular values (or eigenvalues) of matrix $\boldsymbol{A}$, respectively.

where $\boldsymbol{K}_I$, $\boldsymbol{K}_x$, $\boldsymbol{D}_x$ and $\boldsymbol{D}_\eta$ are positive definite matrices. We introduce a new virtual motor coordinate $\boldsymbol{\eta}$, which will be illustrated in Section III-C. The task-space position, velocity and acceleration tracking error are denoted as $\tilde{\boldsymbol{x}} := \boldsymbol{f}(\boldsymbol{q}) - \boldsymbol{x}_d$, $\dot{\tilde{\boldsymbol{x}}} = \boldsymbol{J}\dot{\boldsymbol{q}} - \dot{\boldsymbol{x}}_d$, $\ddot{\tilde{\boldsymbol{x}}} = \boldsymbol{J}\ddot{\boldsymbol{q}} + \dot{\boldsymbol{J}}\dot{\boldsymbol{q}} - \ddot{\boldsymbol{x}}_d$, respectively. $\tilde{\boldsymbol{\lambda}} := \boldsymbol{\lambda} - \boldsymbol{\lambda}_d$ denotes the force tracking error.

In order to achieve the first goal for motion control (from (6b) to (7b)), we only extend the task-space dynamics (6b) by adding a positive definite linear spring $\boldsymbol{K}_x$, a positive definite damping term $\boldsymbol{D}_x$ and pseudo feedforward terms ensuring the tracking performance. Besides, in order to express the dynamics only with $\tilde{\boldsymbol{x}}$ and $\boldsymbol{\eta}$, we replace $\boldsymbol{q}$ in (6b) by using an implicit inverse kinematics function $\boldsymbol{G} : \mathbb{R}^{n-m} \to \bar{\mathbb{Q}}$.

$$\boldsymbol{G}(\tilde{\boldsymbol{x}}) := \bar{\boldsymbol{f}}^{-1}(\mathrm{col}[\boldsymbol{0}, \boldsymbol{x}]) - \bar{\boldsymbol{f}}^{-1}(\mathrm{col}[\boldsymbol{0}, \boldsymbol{x}_d]), \tag{8}$$

This inverse function $\bar{\boldsymbol{f}}^{-1}$ exists due to Ass. 3. Note that it is *only* used as presenting the desired closed-loop dynamics (7a), (7b) with the consistent argument $\tilde{\boldsymbol{x}}$. An explicit formulation of $\boldsymbol{G}(\tilde{\boldsymbol{x}})$ is *not required* in the controller design.

Achieving the second goal for force control (from (6a) to (7a)), we notice that an exact force tracking can be realized by fully compensating the cross coupling Coriolis term $\boldsymbol{\mu}_{cx}\dot{\boldsymbol{x}}$ and force disturbance $\boldsymbol{\lambda}_{ext}$ in (6a), if it is a rigid-joint robot (assuming $\boldsymbol{K}(\boldsymbol{\theta} - \boldsymbol{q})$ as a direct control input). However it is challenging for the case of flexible-joint robots, since the intrinsic elastic coupling $\boldsymbol{K}(\boldsymbol{\theta} - \boldsymbol{q})$ is inevitable. With the objective of aiming for a robust design, we refrain from compensating nonlinear terms and feeding back higher-order derivatives ($\dot{\boldsymbol{\lambda}}_{ext}$), which comes at the price of a reduced force tracking performance. In order to alleviate the latter issue, we introduce an integral term with a positive definite gain $\boldsymbol{K}_I$ into (7a) for suppressing constant bias disturbances. Besides, a feedforward term $\boldsymbol{\lambda}_d$ and a pseudo feedforward term $\boldsymbol{\mu}_{cx}\dot{\boldsymbol{x}}_d$ are also added to guarantee the force tracking. By comparing (6a), (6b) with (7a), (7b), the resulting inertial properties, the intrinsic coupling of elastic elements and the motion/force coupling in closed-loop dynamics are totally preserved. At last, from (1b) to (7c), for better rejecting the motor-side disturbance, we add a positive definite damping $\boldsymbol{D}_\eta$.

In the following text, we shorten the notation and denote a new elastic torque as $\boldsymbol{\psi}(\boldsymbol{\eta}, \tilde{\boldsymbol{x}}) := \boldsymbol{K}(\boldsymbol{\eta} - \boldsymbol{G}(\tilde{\boldsymbol{x}}))$ and an extended reference as $\bar{\boldsymbol{x}}_d := \mathrm{col}[\boldsymbol{0}, \boldsymbol{x}_d]$.

## B. Equilibrium

In order to acquire a first-oder dynamics for a state-space formulation, we take derivative of (7a), and get

$$\dot{\tilde{\boldsymbol{\lambda}}} + \boldsymbol{K}_I\tilde{\boldsymbol{\lambda}} = \boldsymbol{h}_2(\tilde{\boldsymbol{x}}, \dot{\tilde{\boldsymbol{x}}}, \boldsymbol{\eta}, \dot{\boldsymbol{\eta}}) - \dot{\boldsymbol{\lambda}}_{ext}, \tag{9}$$

where[4] $\boldsymbol{h}_2 = \boldsymbol{\mu}_{cx}\ddot{\tilde{\boldsymbol{x}}} + \dot{\boldsymbol{\mu}}_{cx}\dot{\tilde{\boldsymbol{x}}} - \frac{\mathrm{d}}{\mathrm{d}t}\big[(\boldsymbol{A}^{M+})^T\boldsymbol{\psi}(\boldsymbol{\eta}, \tilde{\boldsymbol{x}})\big]$. By defining a state vector $\boldsymbol{z} = \mathrm{col}[\tilde{\boldsymbol{x}}, \dot{\tilde{\boldsymbol{x}}}, \boldsymbol{\eta}, \dot{\boldsymbol{\eta}}, \tilde{\boldsymbol{\lambda}}]$ and imposing $\dot{\boldsymbol{z}} = \boldsymbol{0}$, $\boldsymbol{F}_{ext} = \boldsymbol{0}$ and $\dot{\boldsymbol{\lambda}}_{ext} = \boldsymbol{0}$ on (7a)–(7c), we have

$$\boldsymbol{K}_I\tilde{\boldsymbol{\lambda}} = \boldsymbol{0},\ \boldsymbol{\psi}(\boldsymbol{\eta}, \tilde{\boldsymbol{x}}) = \boldsymbol{0},\ \boldsymbol{K}\tilde{\boldsymbol{x}} = [\boldsymbol{P}(\boldsymbol{J}\boldsymbol{P})^+]^T\boldsymbol{\psi}(\boldsymbol{\eta}, \tilde{\boldsymbol{x}}). \tag{10}$$

It can be easily derived that $\tilde{\boldsymbol{\lambda}} = \boldsymbol{0}$ and $\tilde{\boldsymbol{x}} = \boldsymbol{0}$. The second equation is equivalent to $\boldsymbol{K}(\boldsymbol{\eta} - \boldsymbol{G}(\tilde{\boldsymbol{x}})) = \boldsymbol{0}$. Substituting $\tilde{\boldsymbol{x}} = \boldsymbol{0}$ into (8) leads to $\boldsymbol{G}(\boldsymbol{0}) = \boldsymbol{0}$. Therefore, we have $\boldsymbol{\eta} = \boldsymbol{0}$. The unique equilibrium is the origin, i.e., $\boldsymbol{z} = \boldsymbol{0}$.

[4]Note that since $\ddot{\tilde{\boldsymbol{x}}}$ can be substituted by (7b), $\boldsymbol{h}_2$ is only position- and velocity-dependent.

## C. Coordinate Transformation

The first step is coordinate transformation $(\boldsymbol{x}, \boldsymbol{\theta}) \mapsto (\boldsymbol{x}, \boldsymbol{\eta})$. To achieve the desired closed-loop dynamics, we define a new virtual motor coordinate $\boldsymbol{\eta}$ which imposes the equivalence of (6a), (6b) and (7a), (7b).

$$\boldsymbol{K}(\boldsymbol{\theta} - \boldsymbol{q}) := \boldsymbol{K}(\boldsymbol{\eta} - \boldsymbol{G}(\tilde{\boldsymbol{x}})) + \boldsymbol{n}, \tag{11a}$$

$$\begin{aligned}\boldsymbol{n} = \boldsymbol{A}^T\big[ &-\boldsymbol{\lambda}_d + \boldsymbol{K}_I\int_0^t \tilde{\boldsymbol{\lambda}}(\tau)\mathrm{d}\tau + \boldsymbol{\mu}_{cx}\dot{\boldsymbol{x}}_d\big] \\ &+ (\boldsymbol{J}\boldsymbol{P})^T\big[\boldsymbol{\Lambda}_x\ddot{\boldsymbol{x}}_d + \boldsymbol{\mu}_{xx}\dot{\boldsymbol{x}}_d - \boldsymbol{K}_x\tilde{\boldsymbol{x}} - \boldsymbol{D}_x\dot{\tilde{\boldsymbol{x}}}\big] + \boldsymbol{g},\end{aligned} \tag{11b}$$

where $\boldsymbol{n}$ consists of three parts: (1) an integral force controller with a feedfoward term $-\boldsymbol{\lambda}_d$ and a pseudo feedfoward $\boldsymbol{\mu}_{cx}\dot{\boldsymbol{x}}_d$, projected by $\boldsymbol{A}^T$; (2) a task-space PD+ controller projected by $(\boldsymbol{J}\boldsymbol{P})^T$; (3) a joint-space gravity compensation $\boldsymbol{g}$. In order to obtain the motor velocity and acceleration transformation accordingly, we need to differentiate (11a)–(11b). Note that when differentiating $\boldsymbol{G}(\tilde{\boldsymbol{x}})$ in the (11a), we will have $\dot{\boldsymbol{G}}(\tilde{\boldsymbol{x}}) = \bar{\boldsymbol{J}}^{-1}\dot{\tilde{\boldsymbol{x}}} - \bar{\boldsymbol{J}}^{-1}\dot{\bar{\boldsymbol{x}}}_d = \boldsymbol{q} - \bar{\boldsymbol{J}}^{-1}\dot{\bar{\boldsymbol{x}}}_d$. Hence, $\dot{\boldsymbol{q}}$ in both sides of the first derivative of (11a) will be eliminated. The original motor velocity and acceleration are written by[5]

$$\dot{\boldsymbol{\theta}} = \dot{\boldsymbol{\eta}} + \boldsymbol{a} + \boldsymbol{K}^{-1}\dot{\boldsymbol{n}}, \quad \ddot{\boldsymbol{\theta}} = \ddot{\boldsymbol{\eta}} + \dot{\boldsymbol{a}} + \boldsymbol{K}^{-1}\ddot{\boldsymbol{n}}, \tag{12}$$

where we define $\boldsymbol{a} := \bar{\boldsymbol{J}}^{-1}\dot{\bar{\boldsymbol{x}}}_d$ and $\dot{\boldsymbol{a}} = -\bar{\boldsymbol{J}}^{-1}\dot{\bar{\boldsymbol{J}}}\bar{\boldsymbol{J}}^{-1}\dot{\bar{\boldsymbol{x}}}_d + \bar{\boldsymbol{J}}^{-1}\ddot{\bar{\boldsymbol{x}}}_d$, with $\ddot{\bar{\boldsymbol{x}}}_d = \mathrm{col}[\boldsymbol{0}, \ddot{\boldsymbol{x}}_d]$.

## D. Controller Design

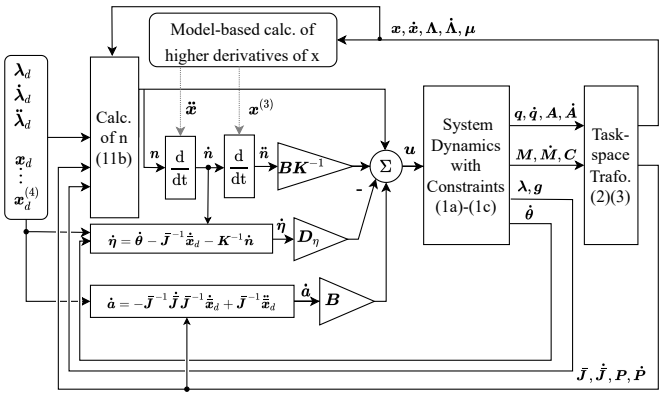


Fig. 1. The proposed control scheme. The block $\frac{\mathrm{d}}{\mathrm{d}t}$ denotes the analytical differentiation of the input signal. The higher derivative is computed by model-based calculation, cf. footnote 5.

By substituting (12) into (1b), we get the intermediate motor dynamics

$$\boldsymbol{B}\ddot{\boldsymbol{\eta}} + \boldsymbol{B}\dot{\boldsymbol{a}} + \boldsymbol{B}\boldsymbol{K}^{-1}\ddot{\boldsymbol{n}} + \boldsymbol{K}(\boldsymbol{\theta} - \boldsymbol{q}) = \boldsymbol{u}. \tag{13}$$

Using (11a)–(11b) and choosing the control input with

$$\boldsymbol{u} = \boldsymbol{B}\boldsymbol{K}^{-1}\ddot{\boldsymbol{n}} + \boldsymbol{B}\dot{\boldsymbol{a}} + \boldsymbol{n} - \boldsymbol{D}_\eta\dot{\boldsymbol{\eta}} \tag{14}$$

lead to the final closed-loop dynamics (7a)–(7c). The proposed control scheme is depicted in Fig. 1. Only gains $\boldsymbol{K}_I$, $\boldsymbol{K}_x$ need to be designed. The damping terms $\boldsymbol{D}_x$, $\boldsymbol{D}_\eta$ are computed by using the modal damping method [17], dependent on the closed-loop inertia, stiffness and the modal factor $\xi$

[5]Note that $\ddot{\boldsymbol{n}}$ includes the jerk $\boldsymbol{x}^{(3)} = \boldsymbol{J}\boldsymbol{q}^{(3)} + 2\dot{\boldsymbol{J}}\ddot{\boldsymbol{q}} + \ddot{\boldsymbol{J}}\dot{\boldsymbol{q}}$, where $\boldsymbol{q}^{(3)}$ is computed by model-based calculation $\boldsymbol{q}^{(3)} = \boldsymbol{M}^{-1}[\boldsymbol{K}(\dot{\boldsymbol{\theta}} - \dot{\boldsymbol{q}}) + \dot{\boldsymbol{A}}^T\boldsymbol{\lambda} + \boldsymbol{A}^T\dot{\boldsymbol{\lambda}} + \dot{\boldsymbol{\tau}}_{ext} - \dot{\boldsymbol{M}}\ddot{\boldsymbol{q}} - \dot{\boldsymbol{C}}\dot{\boldsymbol{q}} - \boldsymbol{C}\ddot{\boldsymbol{q}} - \dot{\boldsymbol{g}}]$, and $\ddot{\boldsymbol{q}} = \boldsymbol{M}^{-1}[\boldsymbol{K}(\boldsymbol{\theta} - \boldsymbol{q}) + \boldsymbol{A}^T\boldsymbol{\lambda} + \boldsymbol{\tau}_{ext} - \boldsymbol{C}\dot{\boldsymbol{q}} - \boldsymbol{g}]$. The constraint force $\boldsymbol{\lambda}$ can be either measured or estimated via $\boldsymbol{\lambda} = (\boldsymbol{A}\boldsymbol{M}^{-1}\boldsymbol{A}^T)^{-1}\boldsymbol{A}\boldsymbol{M}^{-1}[\boldsymbol{C}\dot{\boldsymbol{q}} + \boldsymbol{g} - \boldsymbol{K}(\boldsymbol{\theta} - \boldsymbol{q}) - \boldsymbol{\tau}_{ext}] - (\boldsymbol{A}\boldsymbol{M}^{-1}\boldsymbol{A}^T)^{-1}\dot{\boldsymbol{A}}\dot{\boldsymbol{q}}$.

$(0 \leq \xi \leq 1)$. In general, we chose $\xi = 1$, so that the errors $\tilde{\boldsymbol{x}}$, $\boldsymbol{\eta}$ are critically damped. Hence, $\boldsymbol{K}_x$ (or $\boldsymbol{K}_I$) will affect mostly the convergence rate of $\tilde{\boldsymbol{x}}$, $\boldsymbol{\eta}$ (or $\tilde{\boldsymbol{\lambda}}$).

## IV. Passivity and Stability

In this section, passivity and stability features of the original system dynamics (1a)–(1c) with the proposed controller (14) will be illustrated.

### A. Output Strict Passivity (OSP)

Consider a storage function for (7b)–(7c), written as

$$S = \frac{1}{2}\dot{\tilde{\boldsymbol{x}}}^T \boldsymbol{\Lambda}_{xx} \dot{\tilde{\boldsymbol{x}}} + \frac{1}{2}\dot{\boldsymbol{\eta}}^T \boldsymbol{B} \dot{\boldsymbol{\eta}} + \frac{1}{2}\tilde{\boldsymbol{x}}^T \boldsymbol{K}_x \tilde{\boldsymbol{x}} + U_e(\boldsymbol{\eta} - \boldsymbol{G}(\tilde{\boldsymbol{x}})), \quad (15)$$

where $U_e(\boldsymbol{\eta} - \boldsymbol{G}(\tilde{\boldsymbol{x}})) = \frac{1}{2}(\boldsymbol{\eta} - \boldsymbol{G}(\tilde{\boldsymbol{x}}))^T \boldsymbol{K}(\boldsymbol{\eta} - \boldsymbol{G}(\tilde{\boldsymbol{x}}))$ denotes the potential energy of the elastic element in the closed loop.

**Proposition 1.** *The closed-loop system* (7b)–(7c) *is an output strictly passive map from input* $\boldsymbol{F}_{ext}$ *to output* $\dot{\tilde{\boldsymbol{x}}}$.

*Proof.* As mentioned before, we have $\dot{\boldsymbol{G}}(\tilde{\boldsymbol{x}}) = \bar{\boldsymbol{J}}^{-1}\mathrm{col}[\boldsymbol{0}, \dot{\tilde{\boldsymbol{x}}}]$. Therefore, the effective power flow due to elastic element is[6]

$$\dot{\boldsymbol{G}}^T \boldsymbol{\psi} = \begin{bmatrix} \boldsymbol{0}^T & \dot{\tilde{\boldsymbol{x}}}^T \end{bmatrix} \begin{bmatrix} (\boldsymbol{A}^{M+})^T \\ [\boldsymbol{P}(\boldsymbol{J}\boldsymbol{P})^+]^T \end{bmatrix} \boldsymbol{\psi} = \dot{\tilde{\boldsymbol{x}}}^T [\boldsymbol{P}(\boldsymbol{J}\boldsymbol{P})^+]^T \boldsymbol{\psi}. \quad (16)$$

Take the time derivative of (15) and substitute by (16), $\boldsymbol{\Lambda}_{xx}\ddot{\tilde{\boldsymbol{x}}} = \ldots$ in (7b), $\boldsymbol{B}\ddot{\boldsymbol{\eta}} = \ldots$ in (7c) and $\dot{\boldsymbol{\Lambda}}_{xx} = \boldsymbol{\mu}_{xx} + \boldsymbol{\mu}_{xx}^T$, we get $\dot{S} = \dot{\tilde{\boldsymbol{x}}}^T \boldsymbol{F}_{ext} - \dot{\tilde{\boldsymbol{x}}}^T \boldsymbol{D}_x \dot{\tilde{\boldsymbol{x}}} - \dot{\boldsymbol{\eta}}^T \boldsymbol{D}_\eta \dot{\boldsymbol{\eta}} \leq \dot{\tilde{\boldsymbol{x}}}^T \boldsymbol{F}_{ext}$. □

*Remark*: For the regulation case $\dot{\boldsymbol{x}}_d = \boldsymbol{0}$, the term $\dot{\tilde{\boldsymbol{x}}}^T \boldsymbol{F}_{ext}$ represents the physical power during the interaction.

### B. Uniform Asymptotic Stability (UAS)

The following section shows UAS of the equilibrium when $(\boldsymbol{F}_{ext}, \dot{\boldsymbol{\lambda}}_{ext}) = (\boldsymbol{0}, \boldsymbol{0})$. Note that due to the assumed restriction of non-singular task space, the initial conditions of the task space cannot include the entire space $\boldsymbol{x} \in \mathbb{R}^{n-m}$. Hence, the stability proof is only valid in a local sense [15]. We firstly split the state vector by $\boldsymbol{z} = \mathrm{col}[\boldsymbol{z}_1, \boldsymbol{z}_2] \in \mathbb{R}^{4n-m}$, with $\boldsymbol{z}_1 := \mathrm{col}[\tilde{\boldsymbol{x}}, \dot{\tilde{\boldsymbol{x}}}, \boldsymbol{\eta}, \dot{\boldsymbol{\eta}}] \in \mathbb{R}^{4n-2m}$ and $\boldsymbol{z}_2 := \tilde{\boldsymbol{\lambda}} \in \mathbb{R}^m$. (7a)–(7c) can be written as a first-order system:

$$\frac{\mathrm{d}}{\mathrm{d}t}\begin{bmatrix} \tilde{\boldsymbol{x}} \\ \dot{\tilde{\boldsymbol{x}}} \\ \boldsymbol{\eta} \\ \dot{\boldsymbol{\eta}} \end{bmatrix} = \begin{bmatrix} \dot{\tilde{\boldsymbol{x}}} \\ \boldsymbol{f}_x(t, \tilde{\boldsymbol{x}}, \dot{\tilde{\boldsymbol{x}}}, \boldsymbol{\eta}, \dot{\boldsymbol{\eta}}) \\ \dot{\boldsymbol{\eta}} \\ \boldsymbol{f}_\eta(t, \tilde{\boldsymbol{x}}, \boldsymbol{\eta}, \dot{\boldsymbol{\eta}}) \end{bmatrix} \Leftrightarrow \dot{\boldsymbol{z}}_1 = \boldsymbol{f}_1(t, \boldsymbol{z}_1), \quad (17)$$

$$\frac{\mathrm{d}}{\mathrm{d}t}\tilde{\boldsymbol{\lambda}} = -\boldsymbol{K}_I \tilde{\boldsymbol{\lambda}} + \boldsymbol{h}_2(t, \tilde{\boldsymbol{x}}, \dot{\tilde{\boldsymbol{x}}}, \boldsymbol{\eta}, \dot{\boldsymbol{\eta}}) \Leftrightarrow \dot{\boldsymbol{z}}_2 = \boldsymbol{f}_2(t, \boldsymbol{z}_1, \boldsymbol{z}_2). \quad (18)$$

Hence, (17)–(18) can be seen as a hierarchical system (cf. [18, eq. (2.2)]).

**Proposition 2.** *Consider the closed-loop system* (17)–(18) *under Assumptions 1-4, the equilibrium is uniformly asymptotically stable (UAS) when* $(\boldsymbol{F}_{ext}, \dot{\boldsymbol{\lambda}}_{ext}) = (\boldsymbol{0}, \boldsymbol{0})$.

*Proof.* The proof is shown by using Theorem 1 by Vidyasagar [18, Theorem 3.1] in Appendix A.

*Check for Assumptions:* Assumption (A1) in Theorem 1 is naturally fulfilled when introducing the equilibrium. (A2) is satisfied since $f_i(\cdot,\cdot)$ is continuously differentiable w.r.t. all arguments in some neighborhood of the origin [18, p. 775].

*UAS of* $\boldsymbol{z}_1 = \boldsymbol{0}$ *for the isolated system* (17): By definition, (17) is already isolated. Due to the Matrosov Theorem [19], we can show the UAS of $\boldsymbol{z}_1 = \boldsymbol{0}$. A compact proof is shown in Appendix A.

*UAS of* $\boldsymbol{z}_2 = \boldsymbol{0}$ *for the isolated system* $\dot{\boldsymbol{z}}_2 = \boldsymbol{f}_2(t, \boldsymbol{0}, \boldsymbol{z}_2)$: Substitute $\boldsymbol{z}_1 = \boldsymbol{0}$ into (18) (or (9)), we have $\boldsymbol{h}_2(t, \boldsymbol{z}_1 = \boldsymbol{0}) = \boldsymbol{0}$. Hence the isolated system is simplified as $\dot{\boldsymbol{z}}_2 = -\boldsymbol{K}_I \boldsymbol{z}_2$, implying the UAS straightforward due to the positive definite $\boldsymbol{K}_I$, which completes the proof. □

[6]For the better readability, arguments $\tilde{\boldsymbol{x}}$ in $\boldsymbol{G}(\tilde{\boldsymbol{x}})$, $(\boldsymbol{\eta}, \tilde{\boldsymbol{x}})$ in $\boldsymbol{\psi}(\boldsymbol{\eta}, \tilde{\boldsymbol{x}})$ are neglected in the following text.

## V. Example: A Constrained Two-arm System

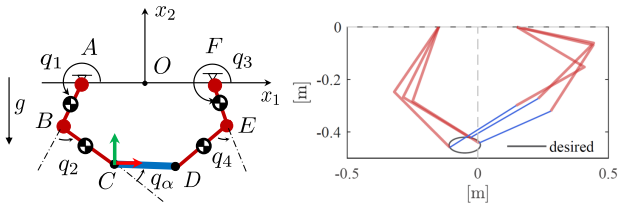


Fig. 2. (a): The constrained two-arm system features SEAs (in large red dots). The four rigid links (red bars) have evenly distributed mass, i.e., CoM locates in the geometric middle point, $\boldsymbol{m_{AB}} = \boldsymbol{m_{EF}} = \boldsymbol{6}$ kg, $\boldsymbol{m_{BC}} = \boldsymbol{m_{DE}} = \boldsymbol{1}$ kg. The motion of two manipulators is constrained by a massless rigid bar. The length of all bars is $\boldsymbol{0.3}$ m. (b): The sequence of different configurations with an ellipse reference trajectory in black.

Consider a planar two-arm system with one kinematic constraint, whose joints implemented by SEAs (all with the same stiffness $K_i = 800$ Nm/rad for all $i = 1, .., 4$, where $K_i$ is $i$-th entry of the diagonal $\boldsymbol{K}$). The unconstrained system has $n = 4$ DoFs in total. By imposing a constraint $\phi(\boldsymbol{q}) = \|\boldsymbol{x}_C(\boldsymbol{q}) - \boldsymbol{x}_D(\boldsymbol{q})\| = \text{const}$ on two end-effectors $C$ and $D$ with a massless rod ($m = 1$), we have the remaining DoF (equal to task space dimension) $n - m = 3$. Hence, $\lambda$ implies the reaction force (or a manipulation force) along this rod. The task space is defined by the Cartesian position and orientation of $C$, i.e., $\boldsymbol{x} = \mathrm{col}[f_x(\boldsymbol{q}),\ f_y(\boldsymbol{q}),\ q_1 + q_2 + q_\alpha(\boldsymbol{q})]$. The schematic diagram is shown in Fig. 2. The desired motion and force trajectories are defined as follows:

(1) The position of the left end-effector follows a frequency-varying ellipse trajectory (at least $C^4$). $\boldsymbol{x}_d(t) = \begin{bmatrix} r_a \cos[\omega(t) \cdot t] + c_a \\ r_b \sin[\omega(t) \cdot t] + c_b \\ \Delta\alpha_0 \sin(\omega_0 \cdot t) + \alpha_0 \end{bmatrix}$, where $\omega(t) = \frac{\Delta\omega_0}{1 + \exp(-(t - h_0))} + \omega_0$, $r_a = 0.06$ m, $r_b = 0.03$ m, $c_a = -0.05$ m, $c_b = -0.45$ m, $\alpha_0 = 6.64$ rad, $\Delta\alpha = 0.2$ rad, $\Delta\omega_0 = 2.5\pi$ rad/s, $\omega_0 = 0.2\pi$ rad/s, $h_0 = 4$ s.

(2) The constrained force should follow with a sinusoid signal (at least $C^2$), i.e., $\lambda_d(t) = \lambda_0 \sin(\omega_\lambda \cdot t)$, where $\lambda_0 = 10$ N, $\omega_\lambda = 2\pi$ rad/s. The gain is chosen by $\boldsymbol{K}_x = \mathrm{diag}(5e3, 5e3, 1e3)$ in N/m, N/m and Nm/rad, $K_I = 10$.

Before starting each simulation, the dynamics initializes with the correct constraint condition $\boldsymbol{\phi}(\boldsymbol{q}) = \boldsymbol{0}$. Besides, we generate disturbances in both spaces with following functions: $\lambda_{ext}(t) = \begin{cases} \frac{a_0}{\sigma_0\sqrt{2\pi}} e^{-0.5 \cdot (\frac{t - h_0}{\sigma_0})^2} & \text{if } t < h_0 \\ a_0 & \text{if } t \geq h_0 \end{cases}$, $\boldsymbol{F}_{ext}(t) =$

$\begin{bmatrix} a_1 \\ a_2 \\ a_3 \end{bmatrix} \frac{1}{\sigma_1\sqrt{2\pi}} e^{-0.5\cdot(\frac{t-h_1}{\sigma_1})^2} \cdot \sin(\omega_e \cdot t)$, where $a_0 = 20$ N, $a_1 = -20$ N, $a_2 = 40$ N, $a_3 = 10$ Nm, $h_0 = 8.0$ s, $h_1 = 6.5$ s, $\sigma_0 = 0.4$, $\sigma_1 = 0.5$, $\omega_e = \pi$ rad/s. Note that at $t = h_0$ s, $\lambda_{ext}(t)$ is $\mathcal{C}^1$-continuous, and $\boldsymbol{F}_{ext}(t)$ fulfills naturally $\mathcal{C}^1$-continuity due to the sine and exponential functions. The disturbances are depicted in the last row of Fig. 3 during the following phases (cf. Fig. 3, those areas with color background):

a. Time 0.0–5.0s: no disturbance;
b. Time 5.0–6.5s (yellow): disturbance $\boldsymbol{F}_{ext}$ appears only in the unconstrained space;
c. Time 6.5–8.0s (lime): disturbances $\boldsymbol{F}_{ext}$ and $\boldsymbol{\lambda}_{ext}$ in both constrained and unconstrained spaces;
d. Time 8.0–10.0s (grey): disturbance $\boldsymbol{\lambda}_{ext}$ purely in the constrained space.

The simulations are performed in MATLAB & SIMULINK using a Runge-Kutta45 solver with fixed step 1 ms.

### A. Results and Discussions

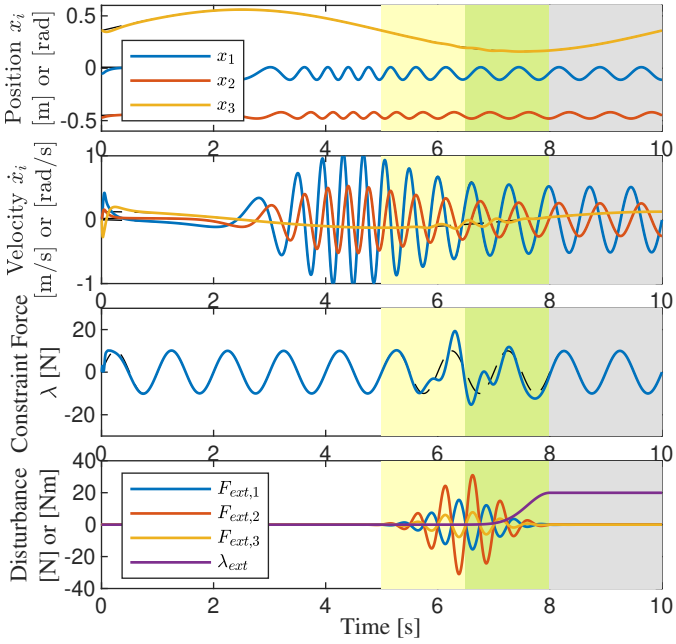


Fig. 3. In the first three rows, the reference trajectories are in dashed black lines, and the actual ones in color lines for position, velocity and constraint force. The last row includes $\boldsymbol{F_{ext,1}}$, $\boldsymbol{F_{ext,2}}$ and $\boldsymbol{F_{ext,3}}$ representing two translational (in $\boldsymbol{x_1}$ and $\boldsymbol{x_2}$) and one rotational (in $\boldsymbol{x_3}$) disturbances. $\boldsymbol{\lambda_{ext}}$ denotes the disturbance in the constrained space.

We have the following observations:

*Phase a (white)*: The task space error (the 1st-2nd row of Fig. 4) is critically damped from the initial error.

*Phase b (yellow)*: The disturbance $\boldsymbol{F}_{ext}$ affects the dynamics in both constrained and unconstrained spaces, cf. the 1st-3rd row of Fig. 4. The stored energy $S$ of the closed loop increases due to the task-space disturbance.

*Phase c (lime)*: With the increasing disturbance $\dot{\lambda}_{ext} \neq 0$, the task space neither is affected nor causes the increase of the system energy cf. the last row in Fig. 4. The disturbance in the constrained space will not inject energy to the closed-loop system, and only the task-space disturbance will do.

*Phase d (grey)*: The constant disturbance $\lambda_{ext} = 20$ N in the constrained space is compensated via the designed integral term (cf. the constraint force error converges to zero in Fig. 4). Same with the observation in Phase c, the disturbance in the constrained space will not cause an energy increase. In the absence of the task-space disturbance $\boldsymbol{F}_{ext}$, the previous injected energy has dissipated due to the passive closed loop.

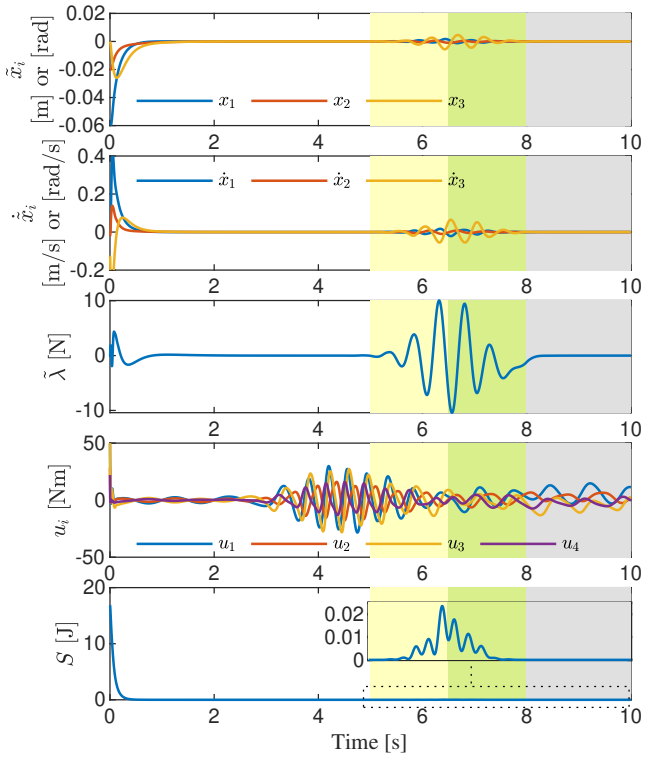


Fig. 4. The first three rows present position $\tilde{\boldsymbol{x}}$, velocity $\dot{\tilde{\boldsymbol{x}}}$ and constraint force $\tilde{\boldsymbol{\lambda}}$ tracking error, respectively. The fourth row shows the control input $\boldsymbol{u}$. The last row depicts the storage function $\boldsymbol{S}$.

## VI. Conclusion

This letter proposed a task-space motion and force tracking controller for constrained elastic joint robots. Different from conventional inverse dynamics [3], [20] or the control that fully decouples motion/force, the proposed controller preserved intrinsic inertial and elastic properties of the system. Due to the passive design, the robustness of the closed-loop system is increased. Meanwhile, instead of compensating nonlinear terms, the force controller part incorporates an integral term that guarantees the force tracking accuracy when encountering a constant disturbance. Without task-space disturbance, the origin of the close loop is uniformly asymptotically stable, even in the presence of a constant disturbance in the constrained space. In the future, experiments of the dual-arm manipulation (a closed-loop kinematic chain) on an elastic system with nonlinear elastic joints, e.g., DLR anthropomorphic robot *David* will be performed.

## APPENDIX

**Theorem 1.** *Vidyasagar [18, Theorem 3.1]: We shall consider the system* (17)–(18) *in a hierarchical form:* $(\mathscr{S})$ $\dot{z}_i = f_i(t, z_1(t), ..., z_i(t)), i = 1, .., n$ *to those of a collection of isolated subsystems* $(\mathscr{S}_i)$ $\dot{z}_i = f_i(t, 0, ..., 0, z_i(t))$. *Suppose the following two assumptions hold: (A1)* $f_i$ *is continuous and* $f_i(t, 0, ..., 0) = 0, \forall t \geq 0, \forall i$ *and (A2) there is a constant* $c$ *such that* $\sup_{t\geq 0} \sup_{\|w_i\|\leq c} \|\nabla_{w_i} f_i(t, w_i)\| < \infty, i = 1, ..., n$, *where* $w_i = \text{col}[z_1, ..z_i]$, *then, the equilibrium* $\boldsymbol{z} = \boldsymbol{0}$ *of* $\mathscr{S}$ *is uniformly asymptotically stable, if and only if* $z_i = 0, \forall i = 1, ..n$ *is a uniformly asymptotically stable equilibrium point of the isolated subsystem* $\mathscr{S}_i$, *for all* $i$.

### A. Proof of UAS for $z_1 = 0$ (via Matrosov's Theorem)

The following proof follows the same procedure as the one in [11]. Since the discussed system in this work is in a task space, only a locally UAS (UGAS in [11]) can be shown. Due to the page limit, we highlight the critical steps, please refer [11] for the complete stability proof in details.

*Proof.* Consider the system (17), where $\boldsymbol{f}_1 : I \times \Omega \to \mathbb{R}^{4n-2m}$ is a continuous function, where $I = [0, \infty)$, and $\Omega$ is an open connected set in $\mathbb{R}^{4n-2m}$, containing $\boldsymbol{z}_1 = \boldsymbol{0}$.

We choose the positive definite storage function $S$ as a Lyapunov candidate $V = S(t, \boldsymbol{z}_1)$, cf. (15) for $\dot{\boldsymbol{z}}_1 = \boldsymbol{f}_1(t, \boldsymbol{z}_1)$. Its time derivative $\dot{V} = \dot{S}$ (with $\boldsymbol{F}_{ext} = \boldsymbol{0}$) is a negative semi-definite function, due to positive definite $\boldsymbol{D}_\eta$ and $\boldsymbol{D}_x$.

We invoke Matrosov's Theorem (the version provided by Paden [19]). At first, we need to show $V$ is lower and upper bounded by functions of class $\mathcal{K}$. Choosing $a_z(\|\boldsymbol{z}_1\|) = \frac{1}{2}\big(\lambda_m(\boldsymbol{\Lambda}_{xx})\|\dot{\tilde{\boldsymbol{x}}}\|^2 + \boldsymbol{B}\|\dot{\boldsymbol{\eta}}\|^2 + \lambda_m(\boldsymbol{K}_x)\|\tilde{\boldsymbol{x}}\|^2\big) + U_e(\boldsymbol{\eta} - \boldsymbol{G}(\tilde{\boldsymbol{x}}))$ and $b_z(\|\boldsymbol{z}_1\|) = \frac{1}{2}\big(\lambda_M(\boldsymbol{\Lambda}_{xx})\|\dot{\tilde{\boldsymbol{x}}}\|^2 + \boldsymbol{B}\|\dot{\boldsymbol{\eta}}\|^2 + \lambda_M(\boldsymbol{K}_x)\|\tilde{\boldsymbol{x}}\|^2\big) + U_e(\boldsymbol{\eta} - \boldsymbol{G}(\tilde{\boldsymbol{x}}))$, then according to [21, Lemma 4.3], there exist class $\mathcal{K}$ functions $a$, $b$ such that $a(\|\boldsymbol{z}_1\|) \leq a_z(\boldsymbol{z}_1)$, $b(\|\boldsymbol{z}_1\|) \geq b_z(\boldsymbol{z}_1)$. Hence, we can conclude $\boldsymbol{z}_1 = \boldsymbol{0}$ is uniformly stable (US) and that Condition (1) in Matrosov's Theorem is fulfilled. It further implies the state variable $\boldsymbol{z}_1$ is bounded. Choose $V^* = -\lambda_M(\boldsymbol{D}_x)\|\dot{\tilde{\boldsymbol{x}}}\|^2 - \dot{\boldsymbol{\eta}}^T\boldsymbol{D}_\eta\dot{\boldsymbol{\eta}}$, then the critical set $E$, where $V^* = 0$, is $E := \{\boldsymbol{z}_1 \in \Omega : \dot{\tilde{\boldsymbol{x}}} = \boldsymbol{0}, \dot{\boldsymbol{\eta}} = \boldsymbol{0}\}$. We choose the auxiliary function $W(t, \boldsymbol{z}_1) := \dot{V}(t, \boldsymbol{z}_1) = -(2\dot{\tilde{\boldsymbol{x}}}^T\boldsymbol{D}_x\ddot{\tilde{\boldsymbol{x}}} + \dot{\tilde{\boldsymbol{x}}}^T\dot{\boldsymbol{D}}_x\dot{\tilde{\boldsymbol{x}}} + 2\dot{\boldsymbol{\eta}}^T\boldsymbol{D}_\eta\ddot{\boldsymbol{\eta}} + \dot{\boldsymbol{\eta}}^T\dot{\boldsymbol{D}}_\eta\dot{\boldsymbol{\eta}})$. Since $\boldsymbol{z}_1 = \boldsymbol{0}$ is US, we conclude that $|W(t, \boldsymbol{z}_1)|$ is bounded. Therefore, Conditions (2) and (3) are satisfied.

The verification of Condition (4) relies on the Lemma by Paden [19, p.1709]. We differentiate $W$ along (7b)(7c):

$$\dot{W}(t, \boldsymbol{z}_1) = -2\big[\boldsymbol{T}\boldsymbol{\psi} - \boldsymbol{K}_x\tilde{\boldsymbol{x}}\big]^T\boldsymbol{Q}\big[\boldsymbol{T}\boldsymbol{\psi} - \boldsymbol{K}_x\tilde{\boldsymbol{x}}\big] - 2\boldsymbol{\psi}^T\boldsymbol{R}\boldsymbol{\psi}, \quad (19)$$

for all $\boldsymbol{z}_1 \in E$, where $\boldsymbol{T} := (\boldsymbol{P}(\boldsymbol{J}\boldsymbol{P})^+)^T$, $\boldsymbol{Q} := \boldsymbol{\Lambda}_{xx}^{-T}\boldsymbol{D}_x\boldsymbol{\Lambda}_{xx}^{-1} = \boldsymbol{Q}^T > 0$, $\boldsymbol{R} := \boldsymbol{B}^{-T}\boldsymbol{D}_\eta\boldsymbol{B}^{-1} = \boldsymbol{R}^T > 0$. [7] Then, (19) can be formulated in a quadratic form: $\dot{W} = -2\text{col}[\boldsymbol{\psi}, \tilde{\boldsymbol{x}}]^T\boldsymbol{H}\text{col}[\boldsymbol{\psi}, \tilde{\boldsymbol{x}}]$, where

$$\boldsymbol{H}(t, \boldsymbol{z}_1) := \begin{bmatrix} \boldsymbol{T}^T\boldsymbol{Q}\boldsymbol{T} + \boldsymbol{R} & -\boldsymbol{T}^T\boldsymbol{Q}\boldsymbol{K}_x \\ -\boldsymbol{K}_x^T\boldsymbol{Q}\boldsymbol{T} & \boldsymbol{K}_x^T\boldsymbol{Q}\boldsymbol{K}_x \end{bmatrix} = \boldsymbol{Y}\boldsymbol{Y}^T, \quad (20)$$

$$\boldsymbol{Y}(t, \boldsymbol{z}_1) := \begin{bmatrix} \boldsymbol{R}^{1/2} & -\boldsymbol{T}^T\boldsymbol{Q}^{1/2} \\ \boldsymbol{0} & \boldsymbol{K}_x^T\boldsymbol{Q}^{1/2} \end{bmatrix} > 0. \quad (21)$$

[7] The symmetric properties of $\boldsymbol{D}_x$ and $\boldsymbol{D}_\eta$ can be achieved, if we choose modal damping design [17].

It implies $\boldsymbol{H}$ is a positive definite, state- and time-dependent matrix. Hence, we can establish $|\dot{W}(t, \boldsymbol{z}_1)| \geq W^*(\boldsymbol{z}_1) := H_m\|\text{col}[\boldsymbol{\psi}, \tilde{\boldsymbol{x}}]\|^2, \forall \boldsymbol{z}_1 \in E$, where $H_m := \lambda_m(\boldsymbol{Y}(t, \boldsymbol{z}_1)) > 0$. In terms of [21, Lemma 4.3], there exists a function $\gamma$ of class $\mathcal{K}$ such that $|\dot{W}(t, \boldsymbol{z}_1)| \geq \gamma(\|\boldsymbol{z}_1\|)$. Hence, invoking Lemma 1 in [11] ensures that Condition (4) is satisfied. Condition (5) is fulfilled, since $\boldsymbol{z}_1 = \boldsymbol{0}$ is US. This completes the proof. □

## REFERENCES


[1] M. Spong, "On the force control problem for flexible joint manipulators," *IEEE Trans. Automat. Contr.*, vol. 34, no. 1, pp. 107–111, 1989.

[2] J. Mills, "Stability and control of elastic-joint robotic manipulators during constrained-motion tasks," *IEEE Trans. Robot. Automat.*, vol. 8, no. 1, pp. 119–126, 1992.

[3] F. Aghili, "A unified approach for inverse and direct dynamics of constrained multibody systems based on linear projection operator: applications to control and simulation," *IEEE Trans. Robot*, vol. 21, no. 5, pp. 834–849, 2005.

[4] M. Mistry, J. Buchli, and S. Schaal, "Inverse dynamics control of floating base systems using orthogonal decomposition," in *2010 IEEE Int. Conf. Robot. Autom.*, 2010, pp. 3406–3412.

[5] M. Mistry and L. Righetti, "Operational space control of constrained and underactuated systems," in *Robotics*, 06 2011.

[6] V. Ortenzi, M. Adjigble, J. A. Kuo, R. Stolkin, and M. Mistry, "An experimental study of robot control during environmental contacts based on projected operational space dynamics," in *2014 IEEE-RAS Int. Conf. on Humanoid Robots*, 2014, pp. 407–412.

[7] H.-C. Lin, J. Smith, K. K. Babarahmati, N. Dehio, and M. Mistry, "A projected inverse dynamics approach for multi-arm cartesian impedance control," in *2018 Int. Conf. Robot. Autom.*, 2018, pp. 5421–5428.

[8] N. Dehio, J. Smith, D. L. Wigand, P. Mohammadi, M. Mistry, and J. J. Steil, "Enabling impedance-based physical human–multi–robot collaboration: Experiments with four torque-controlled manipulators," *Int. J. Robot. Res.*, vol. 41, no. 1, pp. 68–84, 2022.

[9] A. De Luca and F. Flacco, "Dynamic gravity cancellation in robots with flexible transmissions," in *49th IEEE Conf. Decis. Control (CDC)*, 2010, pp. 288–295.

[10] L. Villani, C. De Wit, and B. Brogliato, "An exponentially stable adaptive control for force and position tracking of robot manipulators," *IEEE Trans. Automat. Contr.*, vol. 44, no. 4, pp. 798–802, 1999.

[11] M. Keppler, D. Lakatos, C. Ott, and A. Albu-Schäffer, "Elastic structure preserving (ESP) control for compliantly actuated robots," *IEEE Trans. Robot*, vol. 34, no. 2, pp. 317–335, 2018.

[12] M. Keppler, C. Ott, and A. Albu-Schäffer, "From underactuation to quasi-full actuation: Aiming at a unifying control framework for articulated soft robots," *Int. J. Robust and Nonlinear Control*, vol. 32, no. 9, pp. 5453–5484, 2022.

[13] M. W. Spong, "Modeling and control of elastic joint robots," *J. Dyn. Syst. Meas. Contr.*, vol. 109, no. 4, pp. 310–318, dec 1987.

[14] N. McClamroch, "Singular systems of differential equations as dynamic models for constrained robot systems," in *Proceedings. 1986 IEEE Int. Conf. on Robot. Autom.*, vol. 3, 1986, pp. 21–28.

[15] G. Antonelli, "Stability analysis for prioritized closed-loop inverse kinematic algorithms for redundant robotic systems," *IEEE Trans. Robot*, vol. 25, no. 5, pp. 985–994, 2009.

[16] C. Ott, *Cartesian Impedance Control of Redundant and Flexible-Joint Robots*. Springer, 2008.

[17] A. Albu-Schäffer, C. Ott, U. Frese, and G. Hirzinger, "Cartesian impedance control of redundant robots: recent results with the dlr-light-weight-arms," in *2003 IEEE Int. Conf. on Robot. Autom.*, vol. 3, 2003, pp. 3704–3709 vol.3.

[18] M. Vidyasagar, "Decomposition techniques for large-scale systems with nonadditive interactions: Stability and stabilizability," *IEEE Trans. Automat. Contr.*, vol. 25, no. 4, pp. 773–779, 1980.

[19] B. Paden and R. Panja, "Globally asymptotically stable 'PD+' controller for robot manipulators," *Int. J. Control*, vol. 47, no. 6, pp. 1697–1712, 1988.

[20] H. K. Khalil, *Nonlinear control*. Pearson Higher Ed, 2014.

[21] W. Khalil and E. Dombre, "Modeling, Identification and Control of Robots," *Appl Mech Rev*, vol. 56, no. 3, pp. B37–B38, 05 2003.